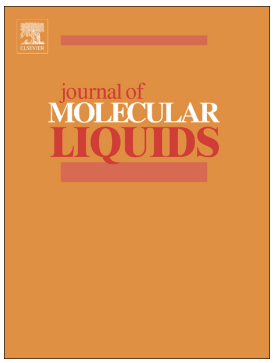

Hierarchical design of hyaluronic acid-peptide constructs for glioblastoma targeting: Combining insights from NMR and molecular dynamics simulations

Maria Mendes, Tânia Cova, João Basso, M. Luísa Ramos, Rui Vitorino, João Sousa, Alberto Pais, Carla Vitorino

PII: S0167-7322(20)32331-X

DOI: https://doi.org/10.1016/j.molliq.2020.113774

Reference: MOLLIQ 113774

To appear in: *Journal of Molecular Liquids*

Received date: 15 April 2020

Revised date: 3 July 2020

Accepted date: 7 July 2020

Please cite this article as: M. Mendes, T. Cova, J. Basso, et al., Hierarchical design of hyaluronic acid-peptide constructs for glioblastoma targeting: Combining insights from NMR and molecular dynamics simulations, *Journal of Molecular Liquids* (2020), https://doi.org/10.1016/j.molliq.2020.113774

Hierarchical design of hyaluronic acid-peptide constructs for glioblastoma targeting: combining insights from NMR and molecular dynamics simulations

Maria Mendes[a,b,c,*], Tânia Cova[c,*], João Basso[a,b,c], M. Luísa Ramos[c], Rui Vitorino[d], João Sousa[a,c], Alberto Pais[c], Carla Vitorino[a,b,c,#]

*These authors contributed equally to this work and should be regarded as co-first authors

[a]Faculty of Pharmacy, University of Coimbra, Polo das Ciências da Saúde, Azinhaga de Santa Comba, 3000-548 Coimbra, Portugal.

[b]Centre for Neurosciences and Cell Biology (CNC), University of Coimbra, Faculty of Medicine, Polo I, 1st floor, Rua Larga, 3004-504 Coimbra, Portugal

[c]Coimbra Chemistry Center, Department of Chemistry, University of Coimbra, Rua Larga, 3004-535 Coimbra, Portugal

[d]Department of Medical Sciences and Institute of Biomedicine – iBiMED, University of Aveiro, Aveiro, Portugal

[#]To whom correspondence should be addressed. (e–mail: csvitorino@ff.uc.pt)

Abstract

The main bottleneck of glioblastoma still relies on the existence of the blood brain-blood brain tumor dual barrier, along with the lack of therapy specificity. The present work deals with the question of whether (and how) different targeting hyaluronic acid (HA)-peptide [c(RGDfK) and/or $H_7K(R_2)_2$] moieties hierarchically interact with each other, to ensure a unique entity with specificity to glioblastoma. A dual experimental-computational approach, encompassing nuclear magnetic resonance and molecular dynamics simulations is enclosed. Relevant contact patterns based on the identification of the stabilizing/destabilizing noncovalent interactions within the constructs are detailed. The synthesis pathway requires the HA-c(RGDfK)-$H_7k(R_2)_2$ association hierarchy, stemming from the size and amino acid residue rearrangement, in the 1:1 molar ratio, to obtain a stable conjugate ultimately able to interact with the tumor cell membrane. To our knowledge, the structural and mechanistic rationale for the formation of hybrid polymer-peptide constructs, including HA-c(RGDfK)-$H_7k(R_2)_2$, for glioblastoma has not been addressed so far.

Keywords: Hyaluronic acid; c(RGDfK; $H_7k(R_2)_2$; polymer-peptide conjugates; glioblastoma

List of abbreviations

HA - Hyaluronic acid

GBM - Glioblastoma

BBB – Blood-brain barrier

ECM- Extracellular matrix

c(RGDfK) - Cyclo (arginine(R)–glycine(G)–aspartic acid(D)–phenylalanine–lysine)

$H_7K(R_2)_2$ - arginine(R)-rich peptide that possesses the pH trigger sequence H_7

CPP - Cell-penetrating peptide

NMR - Nuclear magnetic resonance

MD - Molecular dynamics

EDC - N-(3-Dimethylaminopropyl)-N′-ethylcarbodiimide hydrochloride

sulfo-NHS - N-Hydroxysulfosuccinimide sodium salt

PME - Particle mesh Ewald

IGM - Independent gradient method

RMSD - Root mean square deviation

NCI - Noncovalent interactions

TOCSY - Total correlated spectroscopy

COSY - Correlation spectroscopy

ROESY - Rotating-frame Overhauser spectroscopy

HSQC - Heteronuclear single quantum coherence spectroscopy

HMBC - Heteronuclear Multiple Bond Correlation

HA-c(RGDfK) – Conjugate comprising HA coupled to the c(RGDfK) peptide

HA-c(RGDfK)-$H_7k(R_2)_2$ - Conjugate comprising HA coupled to the $H_7k(R_2)_2$ peptideHA-

c(RGDfK)-$H_7k(R_2)_2$ - Conjugate comprising HA coupled to the c(RGDfK) and $H_7k(R_2)_2$ peptides

HA:c(RGDfK) - Complex established between HA and the c(RGDfK) peptide

HA:$H_7K(R_2)_2$ - Complex established between HA and the $H_7K(R_2)_2$ peptide

HA-c(RGDfK):$H_7k(R_2)_2$ - Complex established between HA-c(RGDfK) conjugate and the $H_7K(R_2)_2$ peptide

1. Introduction

Brain tumors, as heterogeneous malignant neoplasms in the central nervous system, are considered deleterious diseases responsible for incurring a low survival rate. The global estimated number of new cases of brain and other nervous system cancers in 2018 was 3.5 per 100,000 people, while the number of deaths was 2.8 per 100,000 people, which accounts for an 80% mortality rate. Glioblastoma (GBM), a grade IV astrocytoma, arises as the most common, aggressive and lethal malignant brain tumor in humans[1]. The current therapies rely on the surgical resection, followed by radiotherapy and adjuvant chemotherapy[2]. However, the diffuse nature of the tumor hampers an efficient surgical resection, also associated to the inability of removing brainstem structures. The most challenging issues in GBM therapy include the (i) complexity and heterogeneity molecular biology of the tumor, (ii) high growth rate due to the marked angiogenesis contribution, (iii) presence of the blood brain barrier (BBB), a severely restrictive layer, and (iv) structural complexity of the brain, which limits the amount of drugs that achieve therapeutic concentrations in the invasive regions[3]. The armamentarium of strategies currently under investigation, envisioning glioblastoma treatment, is still poorly understood and far from consensual[4–6]. These include, among others, the use of nanosystems, which have been designed aiming at overcoming the limitations and improving the treatment efficacy, ultimately on the basis of a personalized medicine perspective. For that, the functionalization of particle surface to actively targeting the tumor cells and disrupting the tumor microenvironment is mandatory[7]. In this context, and taking advantage of tumor brain related molecular processes, such as transmembrane receptor overexpression (e.g. epidermal growth factor receptors), and the physicochemical tumor features, i.e. lower pH, hypoxia and enzymatic expression, different supramolecular assemblies have been proposed[8–15]. Peptide engineering, involving the residue- and/or site-specific modification of peptides with polymer backbones have been endorsed to design hybrid constructs potentially addressed to fit this purpose.

This work aims at synthesizing a triple targeting polymer-peptide conjugate for the treatment of GBM, mechanistically hypothesized to gather the suitable properties to enhance both tumor targeting and anti-tumor activity. Hyaluronic acid (HA), a component of the extracellular matrix (ECM), and synthesized at the inner face of the plasma membrane as a free linear polymer, is proposed as biopolymer backbone[16]. HA is a biodegradable, biocompatible and a non-immunogenic glycosaminoglycan, composed of repeating disaccharides of

glucuronic acid and N-acetylglucosamine, which has been largely used for tumor targeting[17]. The strategy is supported by the fact that many types of tumor cells, including GBM ones, overexpress HA receptors (e.g. CD44). However, poor selectivity is evidenced, especially due to the facile saturation of CD44. HA:peptide conjugates, including HA:c(RGDfK) and/or HA-c(RGDfK):$H_7k(R_2)_2$ combinations, arise as an interesting approach to improve tumor-specific targeting[18]. Cyclo (arginine(R)–glycine(G)–aspartic acid(D)–phenylalanine–lysine), c(RGDf) peptide is a promising ligand due to the respective high-binding selectivity for αvβ3 and αvβ5 integrins, heterodimeric receptors that mediate tumor growth, metastasis and tumor angiogenesis and are overexpressed on the endothelial cells of tumor angiogenic vessels, as well as in GBM cells (e.g. U-87 MG cell line)[19–21]. In turn, $H_7K(R_2)_2$, an arginine(R)-rich peptide that possesses the pH trigger sequence H_7, can respond to the acidic pH microenvironment in glioma tissues due to the ionization of polyHis switching from hydrophobic to hydrophilic under acid conditions, thus being considered a tumor-specific pH-responsive peptide[22,23]. On the other hand, this peptide presents cell-penetrating peptide (CPP) characteristics, which endow the ability to cross the BBB and to accumulate in the brain in a seemingly energy independent manner. **Figure 1** shows the chemical structures of hyaluronic acid and both peptides, c(RGDfK) and $H_7K(R_2)_2$, as well as potential targeting receptor groups identified through the SwissTargetPrediction server[24].

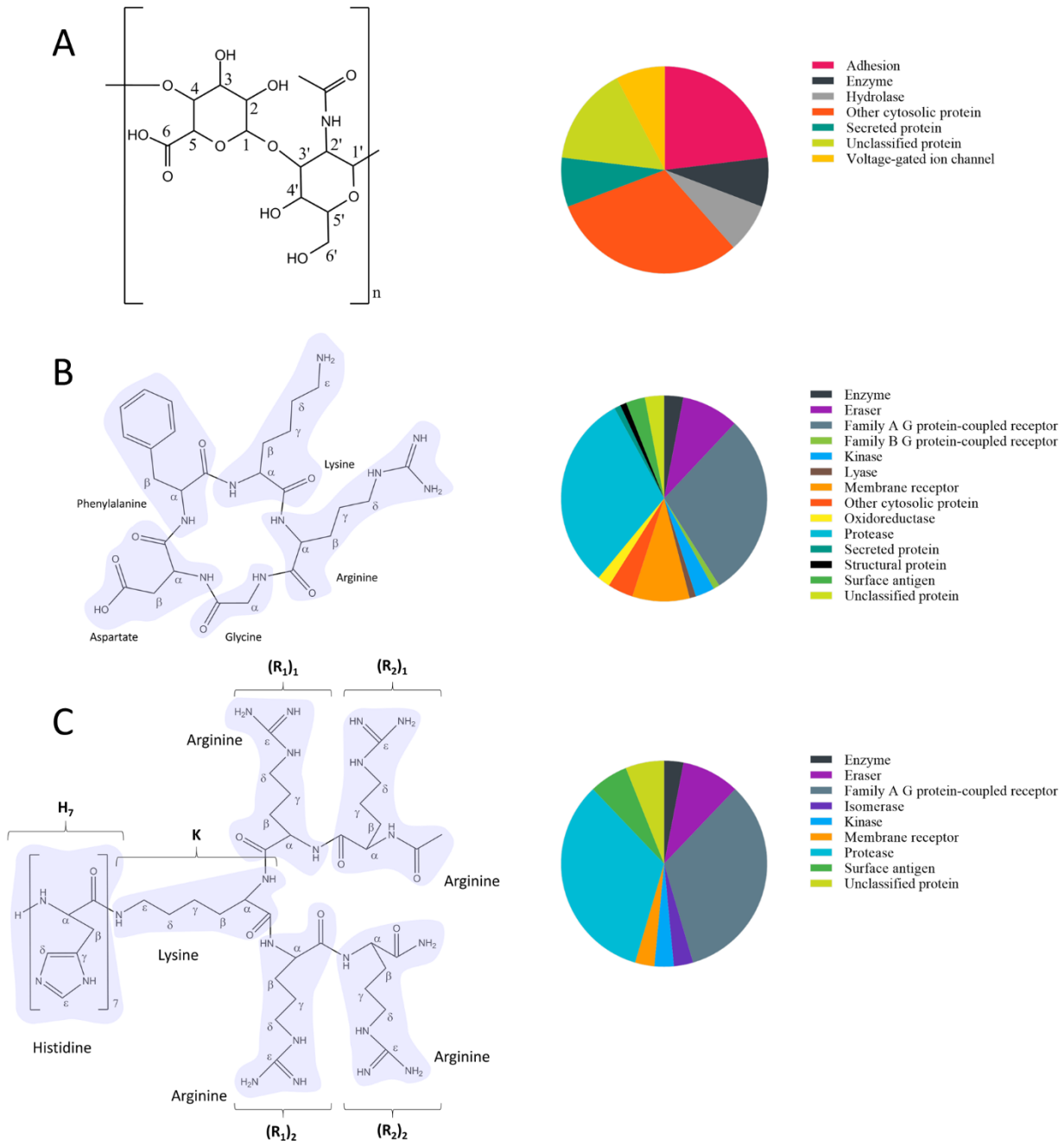

Figure 1. Chemical structures and potential target groups of (A) hyaluronic acid, (B) cyclo (arginine(R)–glycine(G)–aspartic acid(D)–phenylalanine–lysine) c(RGDfK) and (C) $H_7k(R_2)_2$ peptides. For convenience, the C atom and peptide residues labelling for each molecule are included. Note that similarly to MD simulations, the dimer of HA was considered for the target prediction. The "Adhesion" target group refers to the possibility of HA to target enzymes whose interaction may potentially inhibit cancer cell adhesion. (Int. J. Mol. Sci. 2019, 20, 4612; doi:10.3390/ijms20184612).

The synthesis and characterization of polymer-peptide conjugates raise several questions in what concerns the hierarchical topology of such structures. How can the synthesis pathway be tailored to provide a unique stable system? Novelty consists on explaining polymer-peptide interactions based on a dual experimental-computational framework, encompassing nuclear magnetic resonance (NMR) and molecular dynamics (MD) simulations.

1. Materials and methods

2.1.Materials

N-(3-Dimethylaminopropyl)-N′-ethylcarbodiimide hydrochloride (EDC) and N-Hydroxysulfosuccinimide sodium salt (sulfo-NHS) were obtained from Sigma-Aldrich (USA). Hyaluronic acid (MW 14800Da) was acquired from Life Biomedical, LLC (UK). C(RGDfK) and $H_7K(R_2)_2$ were purchased from GL Biochem Ltd (China) and Beijing SciLight Biotechnology LLC (China), respectively.

2.2.Synthesis of peptide-polymer conjugates

Hyaluronic acid (HA) modification was achieved by amine coupling. First, carboxylic groups of HA were activated by EDC/sulfo-NHS method as previously reported[25]. HA ($5x10^{-4}$ mmol) was dissolved in ultrapurified water followed by the addition of EDC ($10x10^{-4}$ mmol) and sulfo-NHS ($10x10^{-4}$ mmol). The reaction mixture was stirred gently for 2 h followed by the addition of c(RGDfK) ($5x10^{-4}$ mmol) and/or $H_7K(R_2)_2$ ($5x10^{-4}$ mmol) and stirring for 3 h. The reaction mixture was dialyzed against ultrapurified water using a 14 kDa cutoff membrane for 24 h to remove unreacted reagents.

2.3.Structural analysis based on NMR

The ^{1}H and ^{13}C NMR spectra were obtained on a Bruker Avance III HD 500 MHz NMR spectrometer. The ^{13}C spectra were recorded using proton decoupling techniques taking advantage of the nuclear Overhauser effect. The methyl signal of *tert*-butyl alcohol was used as internal reference for ^{1}H (δ 1.2) and ^{13}C (δ 31.2) shifts. The homo- and heteronuclear 2D NMR spectra, DQCOSY, TOCSY, ROESY, HSQC and HMBC were recorded on the same spectrometer. Solutions were prepared in D_2O or in a mixture 70% H_2O/30% D_2O and the pH* values quoted are the direct pH-meter readings (room temperature) after standardization with aqueous buffers[26].

2.4.Molecular dynamics simulations

MD simulations combined with the analysis of noncovalent interactions have proven valuable in decoupling the type and strengths of intermolecular interactions, endowing a powerful predictive complement to experiments[27–29]. Aiming at inspecting the experimental synthesis pathway at a molecular level, hierarchical constructs were sequentially analysed, including HA, HA:c(RGDfK), and HA-c(RGDfK):$H_7K(R_2)_2$, based on the topological features of the electronic charge densities of the binding partners. Single solvated peptide molecules were also considered as system references. For HA backbone, two units of glucuronic acid/N-acetylglucosamine were considered. The starting geometries of HA, c(RGDfK), $H_7K(R_2)_2$ and the respective conjugates were constructed in Avogadro and Pymol and optimized with the semi-empirical Antechamber/SQM method. Partial charges for each molecule were obtained from AM1-BCC[30].

A cubic box of 8.5×8.5×8.5 nm^3 was employed for each system containing one molecule of each binding partner HA:c(RGDfK), HA:$H_7K(R_2)_2$, and HA-c(RGDfK):$H_7K(R_2)_2$, solvated with approximately 20200 water molecules.

2.4.1. Simulation details

MD simulations were performed using the GROMACS package (version 4.6.5)[31] and the all atom amber99sb force field[32], under periodic boundary conditions, and with a NPT ensemble, see[33]. TIP3P waters were employed for modelling aqueous solvation. A constant temperature and pressure of 300 K and 1 bar, respectively, were imposed in all simulations, by the coupling constants of 0.5 ps and 1 ps, respectively. An equilibration run of 40 ns was performed prior to each production run, maintaining the pressure at 1 bar. No pressure coupling was imposed during the production runs, allowing to keep the size of the simulation box constant. Lennard–Jones interactions and electrostatic interactions were assessed using a cut-off of 0.9 nm and the particle mesh Ewald (PME) method, respectively[34]. The constraints in the binding partners were imposed by the LINCS algorithm[35].

2.4.2. Analysis of noncovalent interactions

Evaluation of the noncovalent interactions (NCI) within HA:c(RGDfK), HA:$H_7K(R_2)_2$, c(RGDfK):$H_7K(R_2)_2$, and HA-c(RGDfK):$H_7K(R_2)_2$ associations was performed based on the Independent Gradient Method (IGM)[28,36], and using the IGMPlot software (version 1.0). This method is based on the analysis of the electronic charge density of the binding partners and the respective gradients, also enabling the visualization and quantification of those regions of

stabilizing/destabilizing noncovalent interactions. IGM is governed by the topological characteristics of the electronic charge density, ρ, of each system. In addition to ρ, this method uses quantities corresponding to the first and second derivatives of the density. δg^{inter} refers to the IGM descriptor estimated by the difference between the first derivatives of the charge densities for the final system and the respective single components,

$$\delta g^{inter} = \left|\nabla \rho^{IGM,inter}\right| - |\nabla \rho| \qquad \text{(Eq. 1)}$$

The occurrence and strength of noncovalent interactions are inferred, respectively, when $\delta g^{inter} > 0$, and by the magnitude of the descriptor at a point in space.

$\nabla \rho^{IGM,inter}$ is obtained from the sum of the N atoms in the different components, referred as A and B, in the x-direction,

$$\left(\frac{\delta \rho}{\delta x}\right)^{IGM,inter} = \left|\sum_{i=1}^{N_A} \frac{\delta \rho_i}{\delta x}\right| + \left|\sum_{i=1}^{N_B} \frac{\delta \rho_i}{\delta x}\right| \qquad \text{(Eq. 2)}$$

IGMPlot employs the pre-computed atomic charge densities for estimating a pro-molecular density that produces a minimal effect on the noncovalent interactions. δg^{inter} allows identifying NCI regions, and $\nabla^2 \rho$, a second derivative (Laplacian) of the density, is used for discriminating favorable/unfavorable NCIs. The decomposition of the Laplacian term into $\nabla^2\rho=\lambda_1+\lambda_2+\lambda_3$ ($\lambda_1 \leq \lambda_2 \leq \lambda_3$), the three eigenvalues of maximal variation, provides information on the stabilizing ($\lambda_2 < 0$) or destabilizing ($\lambda_2 > 0$) interactions. Larger (negative) values of $sign(\lambda_2)\rho$ indicate stronger interactions, e.g. hydrogen bonds, while values close to zero reflect weak NCI, including van der Waals forces.

The coordinates of the HA:c(RGDfK), HA:$H_7K(R_2)_2$, and HA-c(RGDfK):$H_7K(R_2)_2$ conjugates were extracted from the ensemble of structures at the equilibrium state, sampled during the MD simulations (100 ns of production run), using the clustering procedure described in[33]. Geometric clusters were established based on the calculation of the root mean square deviation (RMSD of 0.25 nm) of the atom positions between all pairs of each polymer-peptide structure. Also, water molecules were discarded and the conjugates were separated into the respective binding components[33]. NCI are represented by isosurface volumes for the δg^{inter}, coloured according to the $sign(\lambda_2)\rho$ values. These values provide a quantitative evaluation of the types and strengths of NCI within each system, reflecting both the extent and (de)stabilizing nature of the interactions.

Visual Molecular Dynamics software version 1.9.2 was used to visualize the polymer-peptide systems and the respective isosurfaces.

3. Results and discussion

The rationale behind polymer-peptide conjugate synthesis is assuming increasingly importance, in particular for tumour targeting purposes. Betting on supramolecular structures that entail a certain level of complexity, associated to e.g. the size, nature and type of amino acid residues, and also to variations in conformational behavior must be supported by a deep understanding of the mechanistic aspects involved in the binding process and stability of polymer-peptide conjugates. In this context, several questions are raised: How can polymer-peptide supramolecular constructs be formed? Is the peptide order addition relevant? What governs these hierarchical constructs at the molecular level? Which are the main interaction forces established? These challenging aspects are explored in what follows, combining insights from NMR and MD simulations.

3.1. Synthetic route proposed for polymer:peptide contructs

The hierarchical design of hyaluronic acid-peptide constructs for glioblastoma targeting is hypothesized in **Figures 2** and **3**. Such proposal results from the successful attachment of c(RGDfK) and $H_7K(R_2)_2$ peptides onto the HA backbone, which enables their further utilization in the surface shaping of ultra-small lipid nanoparticles tailored for glioblastoma targeting. Systems corresponding to HA:c(RGDfK), HA:$H_7K(R_2)_2$, and HA-c(RGDfK):$H_7K(R_2)_2$ interaction pairs will be duly discussed, so as to establish the assumptions for the suggested synthetic route.

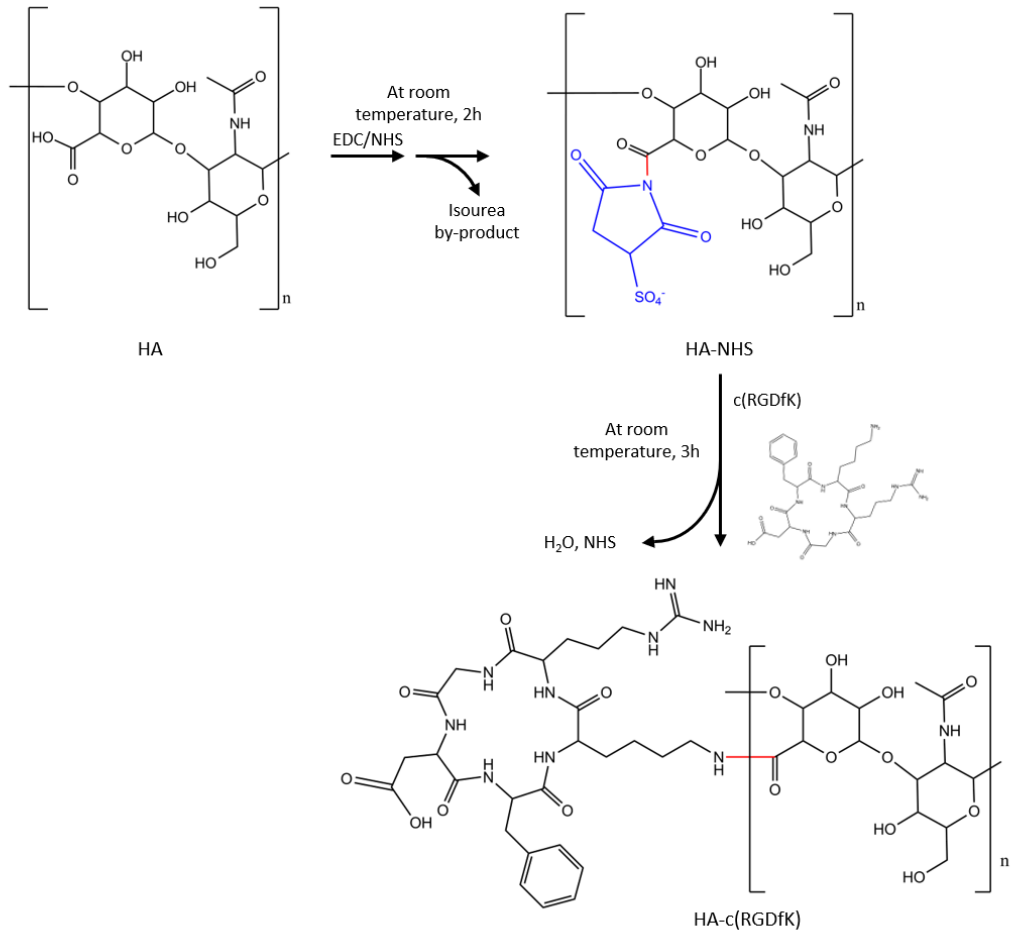

Figure 2. Schematic representation of the synthesis of HA-c(RGDfK). The blue molecule corresponds to NHS required for the HA carboxylic group activation. The red bonds stand for the formation of new covalent bond between molecules.

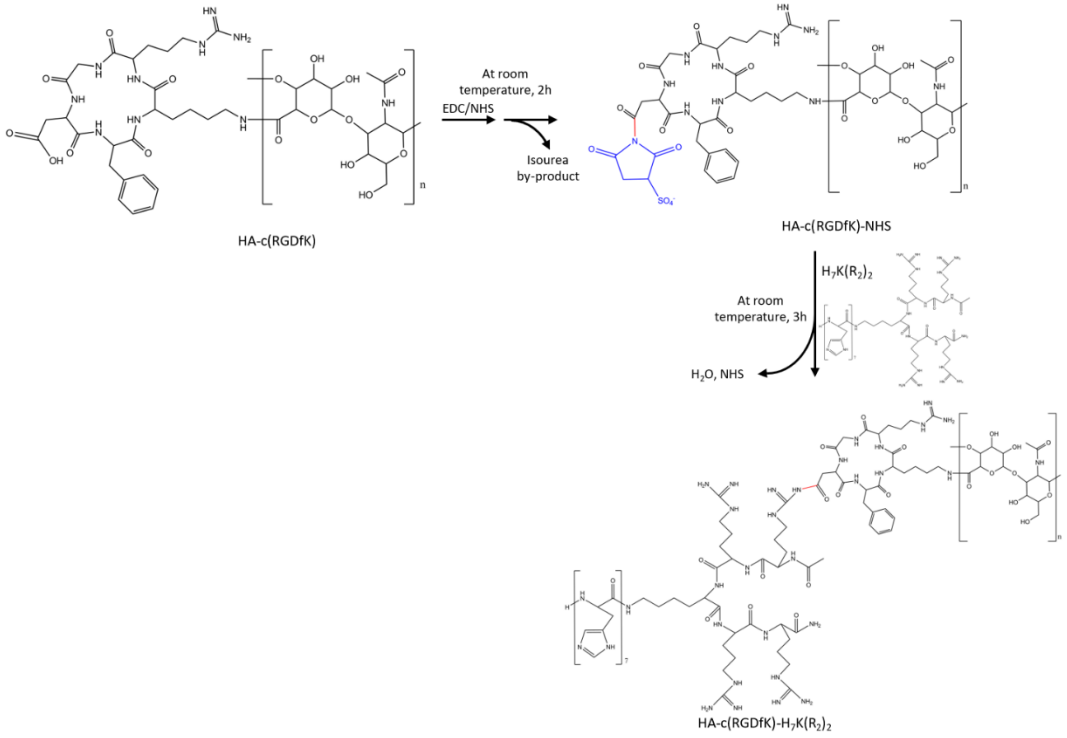

Figure 3. Schematic representation of the formation of HA-c(RGDfK):$H_7K(R_2)_2$ conjugate. The blue molecule corresponds to the NHS required for the c(RGDfK) carboxylic group activation. The red bonds stand to the formation of new covalent bond between molecules.

3.2. Hierarchical construction of peptide conjugates

The type and extent of the interactions between HA, c(RGDfK) and $H_7K(R_2)_2$ are critical for establishing the binding sites, exploring conformational changes, and providing an in-depth knowledge of the dynamics of polymer-peptide conjugation. Such information is only experimentally available when fingerprint techniques, including NMR spectroscopy, are utilized.

HA:c(RGDfK)

The ^{1}H and ^{13}C NMR spectra were first acquired for the individual components, HA and the c(RGDfK) peptide, and for the synthesized conjugate between HA and the peptide in the molar ratio 1:1 in D_2O and D_2O/H_2O solutions. Spectra are presented in **Figures 4 – 6**.

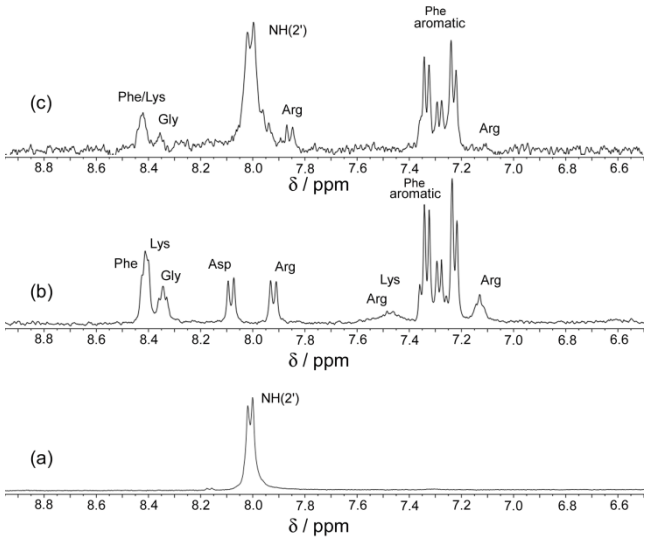

Figure 4. ^{1}H NMR spectra of the NH region (expansion 6.5 – 9.0 ppm) of the solutions in H_2O/D_2O (70%:30%) of (a) hyaluronic acid (HA) 5.0 mmol dm^{-3}, pH* 6.61; (b) c(RGDfK) peptide, 5.0 mmol dm^{-3}, pH* 3.21 and (c) HA-c(RGDfK) conjugate 5.0 mmol dm^{-3}, pH* 3.15.

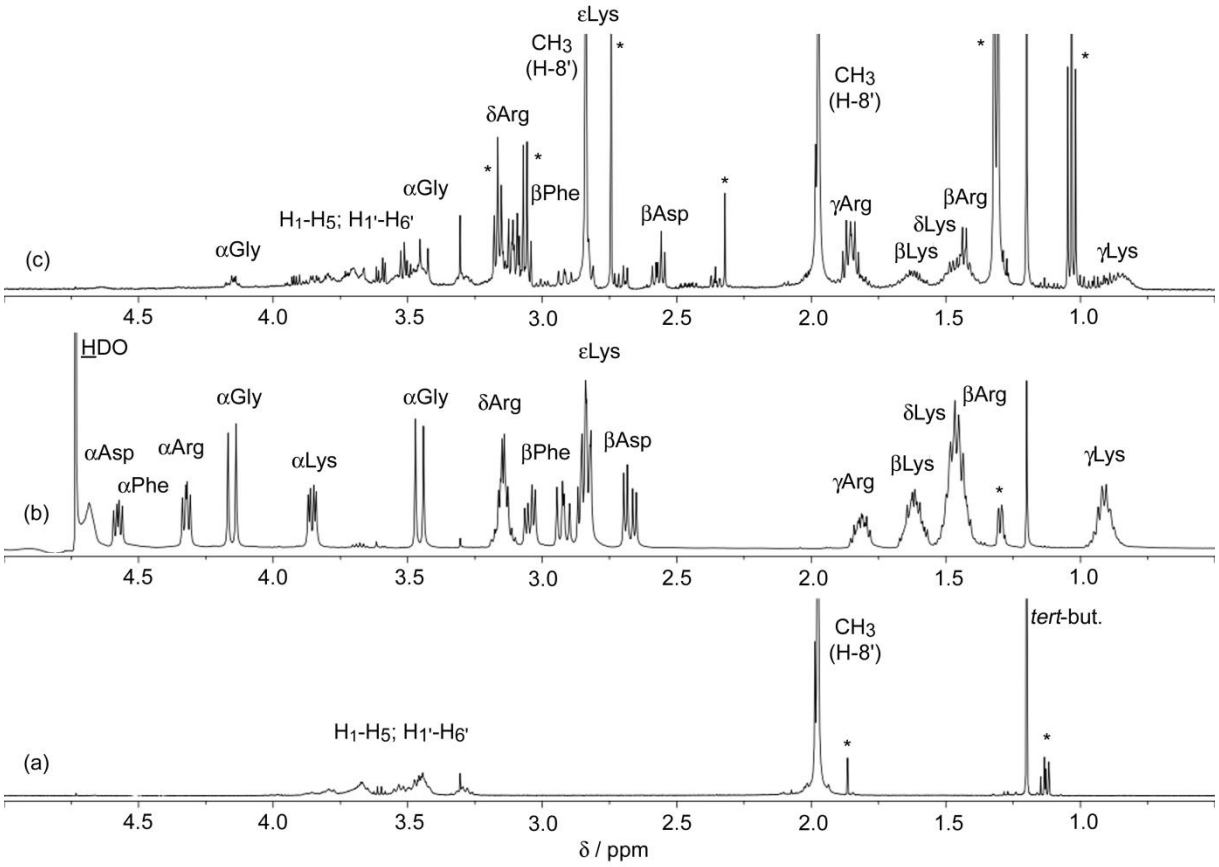

Figure 5. ^{1}H NMR spectra of the C<u>H</u> region (expansion 0.5 – 5.0 ppm) of the solutions in D_2O of (a) hyaluronic acid (HA) 5.0 mmol dm^{-3}, pH* 6.61; (b) c(RGDfK) peptide 5.0 mmol dm^{-3}, pH* 3.13; and (c) HA-c(RGDfK) conjugate 5.0 mmol dm^{-3}, pH* 3.15. *Signals not assigned.

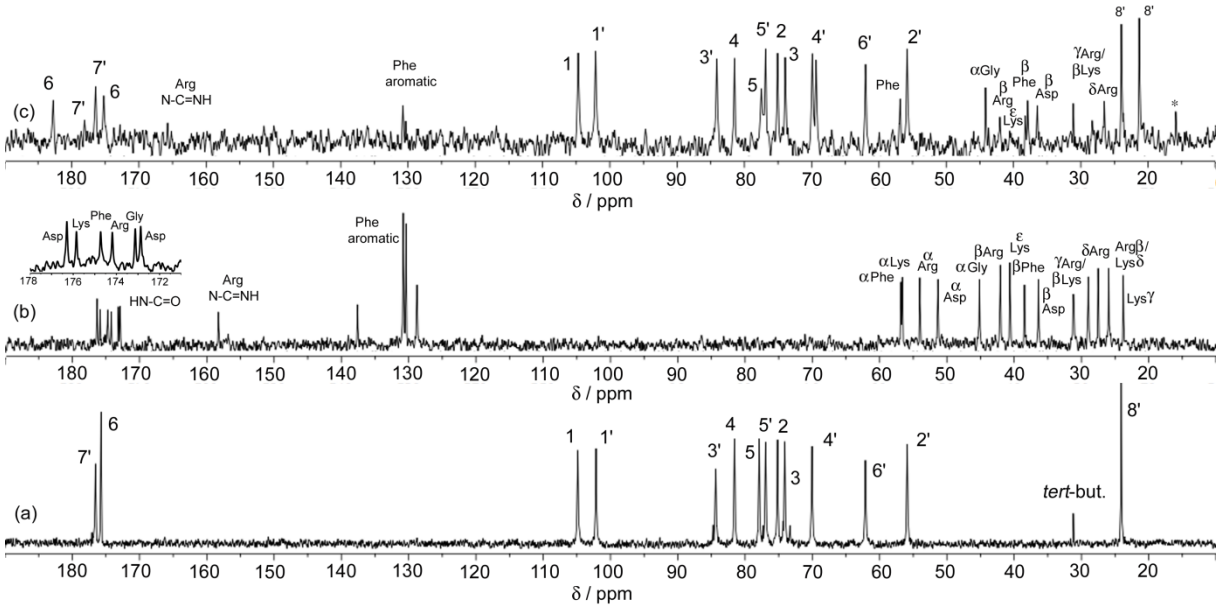

Figure 6. ^{13}C NMR spectra of the solutions in D_2O of (a) hyaluronic acid (HA) 5.0 mmol dm^{-3}, pH* 6.61; (b) c(RGDfK) peptide 5.0 mmol dm^{-3}, pH* 3.13; and (b) HA-c(RGDfK) conjugate, 5.0 mmol dm^{-3}, pH* 3.15. *Signal not assigned.

The assignment of ^{1}H and ^{13}C spectra was completed based on homonuclear and heteronuclear correlations obtained in the bi-dimensional spectra. ^{1}H spin systems were identified based on TOCSY data, starting from NH signals (**Figure S1**), and the ^{1}H NMR signals fully assigned by combining TOCSY with COSY (**Figure S2**) and ROESY spectra. ^{13}C assignment was based on HSQC and HMBC spectra (**Figures S3 and S4**, respectively). The complete ^{1}H spectral parameters are shown in **Tables S1-3**, while the corresponding ^{13}C spectral parameters are shown in **Tables S4 and S5**.

Clear indications of the binding sites were obtained by comparison of induced shifts or linewidth changes of the ^{1}H and ^{13}C signals of each of the molecules in the HA-c(RGDfK) conjugate, with those corresponding to HA and peptide single molecules. Information on conformational variations can be also obtained from broadening/narrowing of the signals, or from changes in the coupling constants of each of the molecules under the same conditions, *viz*[37,38].

For better visualization of the NH region, we show, in Figures 4 and 5, two expansions of the ^{1}H NMR spectra of HA, c(RGDfK) peptide and HA-c(RGDfK) conjugate, the NH and the CH regions, respectively. In both Figures 4 and 5, ^{1}H NMR spectra of HA in the HA-c(RGDfK) conjugate show negligible chemical shift or linewidth changes, except for the methyl group CH_3-8' signal, which displays two signals, with 1:1 intensities ratio (1.97 and 2.84 ppm). This suggests two different electronic environments, one of them similar to free HA and the other showing a significant shift towards higher frequencies, indicating the possibility of the involvement of the methyl group CH_3-8' with the peptide chain. In agreement with this, ^{13}C NMR spectra also show two signals of similar intensity for C-8', and, in addition, show two signals with different intensities for C-7'. Some additional changes are observed in the spectra of the complex, including the appearance of new signals for C-4' and C-6, and a decrease in intensity for C-5, attributed to broadening of the band, which suggest that the carboxylic group of the glucuronic acid moiety may also be involved in interactions with the peptide chain. More marked changes are observed for the ^{1}H and ^{13}C NMR signals of the peptide chain in the presence of HA, where for the majority of the ^{1}H signals are observed to show shifts and/or intensity variations as a result of changes in the linewidth. The spectra in the O=C-N-H region are affected intensely, as can be seen in **Figure 4**, with the signal corresponding to terminal N-H group of lysine being observed to be broadened, strongly suggesting that the terminal NH_2 may be bound to the carboxylic group of HA. In addition, glycine, arginine and phenylalanine are also affected, and decreasing in intensity as a result of the broadening being ascribed to the decrease in the flexibility of the cyclic core of the peptide (**Figure 1**). The same effect is observed for the aromatic region of the phenylalanine, also suggesting an increase of the rigidity of the aromatic ring in the HA-c(RGDfK) conjugate. A pronounced broadening is also seen in the other regions of the spectra, which is most pronounced for the signals of the lysine lateral chain, in particular, the signal of CH_2-ε of lysine, also indicating that its terminal NH_2 may be bound to the carboxylic group of HA (**Figure 5**). This observation is in complete agreement with the loss of the coupling constants (**Table S3**) and the intensity changes observed for the ^{13}C signals of the lysine lateral chain due to the signal broadening (**Figure 6**). Notwithstanding, this interaction is not observed when both single molecules are in solution, due to the rigidity of the HA backbone associated to intramolecular hydrogen bonds between the carboxyl group in C6 and the hydroxyl group in C6'. Likewise, no carboxyl groups remain available to establish interaction with terminal NH_2 of lysine moiety in c(RGDfK). Moreover, the ^{13}C NMR spectra of HA in the presence of the peptide show two signals for each of the carbon atoms C-6 and C-7', one of them shifted to high frequencies and the other one

presenting very similar resonance to the respective nuclei in free HA; in addition, the signals corresponding to nuclei C-5 and C-4' appear broadened and duplicated, respectively (**Figure 6**). These observations, in particular, the intensities of the bound and unbound signals, suggest that spatially alternating moieties of HA are involved in interactions with the peptide by the carboxylic acid, which is bound to the terminal NH_2 group of lysine. This alternating state allows the formation of other NH···O hydrogen bonds between other moieties of c(RGDfK), such as C6=O ··· NH (D-Phe), see **Table S1**.

Additional interactions of the methyl group of the *N*-acetyl glucosamine moiety with the aromatic group of phenylalanine cannot be ruled out, based on the changes in the corresponding signals, as has previously been described for peptides and HA[39].

HA:$H_7K(R_2)_2$

The ^{1}H NMR spectra of HA in the HA-$H_7K(R_2)_2$ conjugate indicate, when compared to free HA, negligible chemical shift or linewidth changes, except for the methyl group C$\underline{H}_3$-8' signal, which displays two signals, (1.97 and 2.83 ppm) with 2:1 and 4:1 intensities ratio, for conjugates synthesised starting from mixtures containing HA-$H_7K(R_2)_2$ with molar ratios 1:1 and 4:1, respectively. Two different electronic environments are suggested, one of them containing two and four units, respectively, similar to free HA, while the other corresponds to one unit, showing a significant shift towards higher frequencies, indicating the possibility of the involvement of the methyl group C$\underline{H}_3$-8' with the peptide. In agreement with this, ^{13}C NMR spectra also show two signals with similar relative intensities for C-8'. Some minor additional changes are observed for HA in the spectra of the conjugate, including a decrease in intensity for C-5, attributed to broadening of the band, which also suggests that the D-glucuronic moiety may also be involved with the $H_7K(R_2)_2$ peptide. Moreover, significant changes of intensity are observed for the carboxyl groups of HA, suggesting the involvement in the peptide binding. More marked changes are also observed for the ^{1}H and ^{13}C NMR signals of the peptide chain in the presence of HA, where for the majority of the ^{1}H and ^{13}C signals are observed significant variations. For most of the signals, the severe broadening precludes their detection, suggesting the increasing of the rigidity of the chain. The conjugate is established probably via the linkage between the carboxylic group of HA and the α-NH group of the terminal histidine residue. In addition, the loss of the ^{1}H and ^{13}C signals should indicate the decrease of the flexibility of the peptide chain, also suggesting an increase of hydrophobic interactions together with important steric effects arising from the HA backbone in the conjugate when compared with the peptide alone. These observations, in particular, the intensities of the bound and unbound signals of

methyl group C<u>H</u>$_3$-8', suggest that in the conjugate obtained from the solution having a HA to peptide molar ratio 1:1, considering three consecutive moieties of HA, two are free and one is involved in interactions with the peptide.

HA-c(RGDfK):$H_7K(R_2)_2$

The HA-c(RGDfK):$H_7K(R_2)_2$ conjugate was subsequently prepared by the addition of $H_7K(R_2)_2$ to the preformed HA-c(RGDfK) in the 1:1 molar ratio. The corresponding ^{1}H and ^{13}C spectra are represented in **Figures 7 d) and 8 d)**. Two ^{1}H signals, (1.97 and 2.84 ppm) for the methyl group C<u>H</u>$_3$-8', corresponding to free and conjugated HA, also show the 2:1 intensities ratio as is observed for the HA conjugate obtained with the peptide $H_7K(R_2)_2$ alone. In agreement with this, ^{13}C NMR spectra also show two signals for C-8'. This observation, together with the presence of ^{1}H and ^{13}C signals of the conjugate of HA-c(RGDfK) (**Figures 7 d) and 8 d), Tables S6-9**), suggests the maintenance of the HA-c(RGDfK). Moreover, a severe broadening occurred by the multiple peptide interactions, and the absence of characteristic ^{1}H and ^{13}C signals of $H_7K(R_2)_2$ reinforces the existence of a strong binding between both peptides, see **Figure 8**. Further insights on the formation of polymer-peptide conjugates were provided by the *in silico* counterpart.

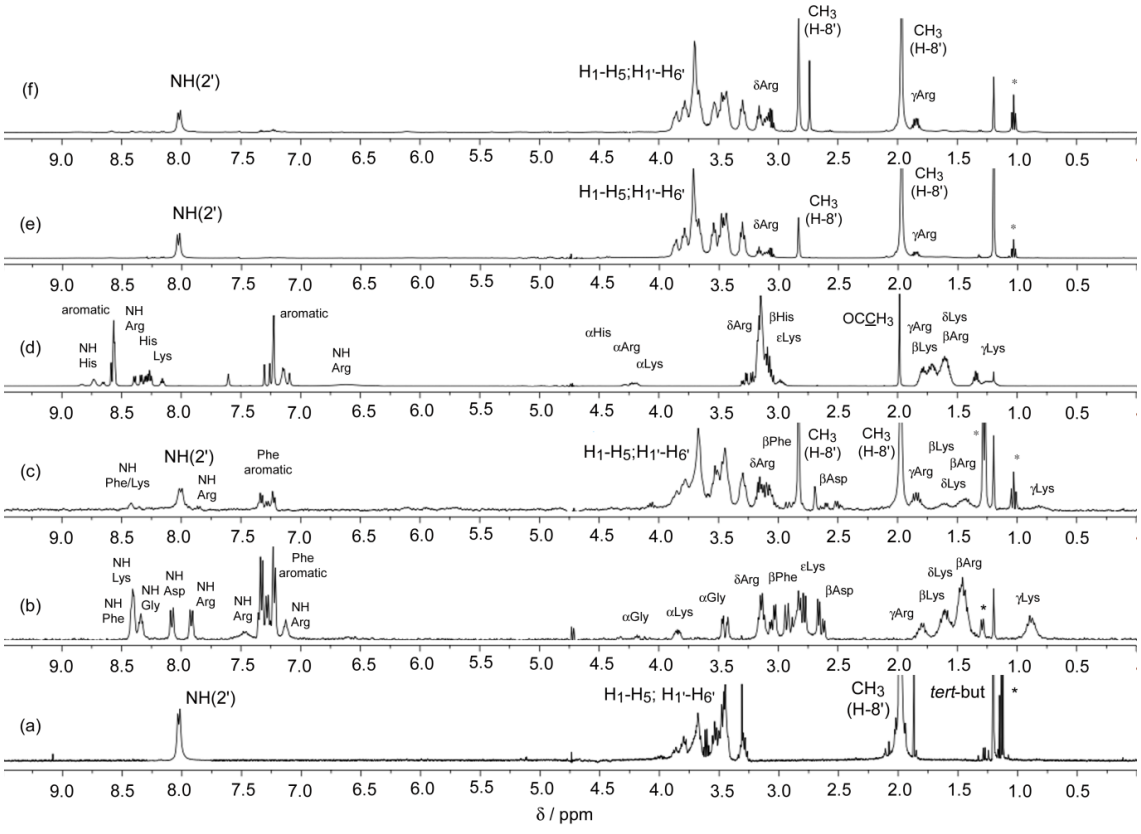

Figure 7. ^{1}H NMR spectra of the solutions in H_2O/D_2O of (a) hyaluronic acid (HA), 5.0 mmol dm^{-3}, pH* 6.61; (b) c(RGDfK) peptide, 5.0 mmol dm^{-3}, pH* 3.13 (c) conjugate of hyaluronic acid and peptide c(RGDfK), HA-c(RGDfK), 5.0 mmol dm^{-3}, pH* 3.15; (d) $H_7K(R_2)_2$ peptide, 5.0 mmol dm^{-3}, pH* 3.15; (e) conjugate of hyaluronic acid and $H_7K(R_2)_2$, HA-($H_7K(R_2)_2$) 5.0 mmol dm^{-3}, pH* 4.20 and (f) conjugate of hyaluronic acid and c(RGDfK) peptide in the presence of the $H_7K(R_2)_2$ peptide, HA-c(RGDfK):$H_7K(R_2)_2$ 5.0 mmol dm^{-3}, pH* 3.88. *Signals not assigned.

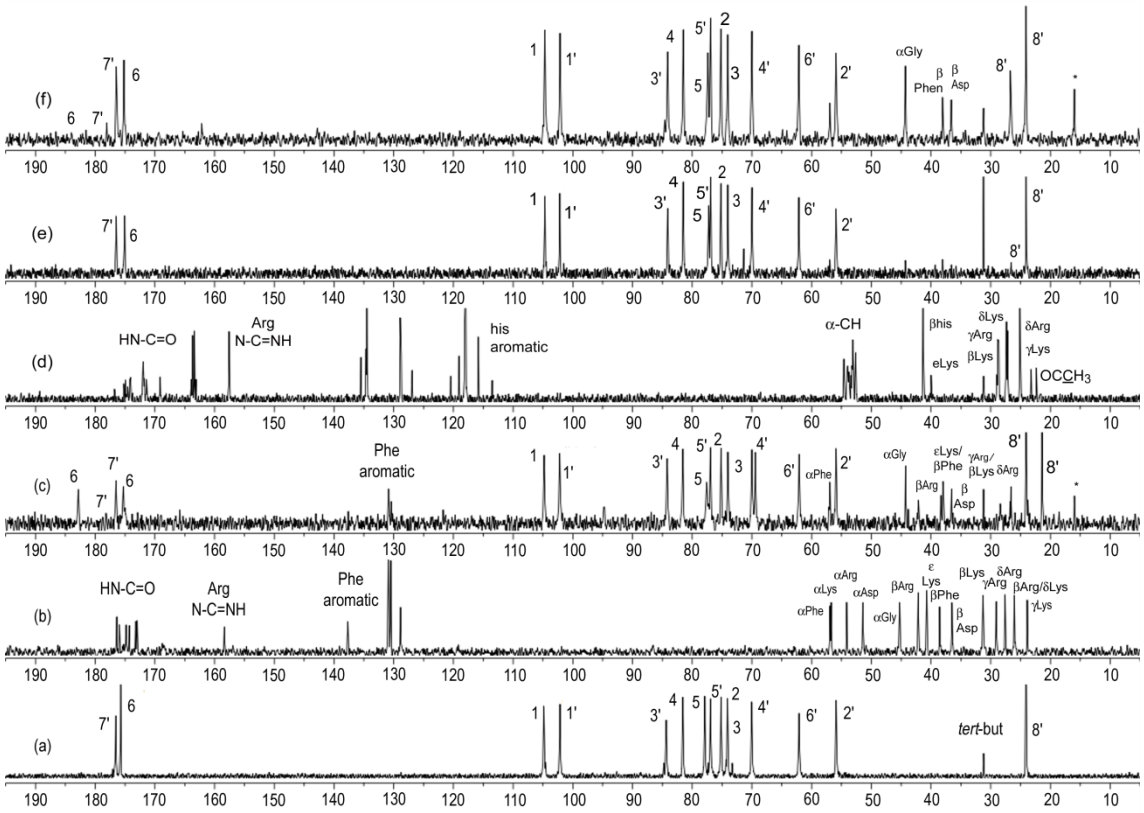

Figure 8. ^{13}C NMR spectra of the solutions in H_2O/D_2O of (a) hyaluronic acid 5 mmol dm^{-3}, pH* 6.61; (b) c(RGDfK) peptide, 5.0 mmol dm^{-3}, pH* 3.13 (c) conjugate of hyaluronic acid and c(RGDfK) peptide, HA-c(RGDfK), 5.0 mmol dm^{-3}, pH* 3.15; (d) $H_7K(R_2)_2$ peptide, 5.0 mmol dm^{-3}, pH* 3.15; (e) conjugate of hyaluronic acid and $H_7K(R_2)_2$ peptide, HA:$H_7K(R_2)_2$, 5.0 mmol dm^{-3}, pH* 4.20 and (f) conjugate of hyaluronic acid and c(RGDfK) peptide in the presence of the $H_7K(R_2)_2$ peptide, HA-c(RGDfK): $H_7K(R_2)_2$ 5.0 mmol dm^{-3}, pH* 3.88.*Signals not assigned.

3.3. Computational rationale for describing HA:peptide constructs

The most favorable noncovalent interactions within the different polymer/peptide scenarios are detailed in **Figure 9**. The volume of the interacting regions within each polymer/peptide association allows inferring on the extent of the interactions of the HA-c(RGDfK)-$H_7K(R_2)_2$ conjugates. Binding specificity is represented by 3D isosurfaces corresponding to discrete regions of enhanced interactions, being influenced by the nature of the peptide residues involved in the interaction. Blue and red denote, respectively, stronger stabilizing and destabilizing interactions, while green indicates van der Waals forces. The asymmetry of the peaks as displayed in the 2D scatter plots (top), reflects the favorable nature of the polymer:peptide interactions. The peaks on the negative stabilizing side of the $sign(\lambda_2)\rho$ axis are more intense than the corresponding ones on the positive destabilizing side, indicating that the balance of noncovalent forces in each polymer/peptide system are prompting the conjugate formation and the respective stability.

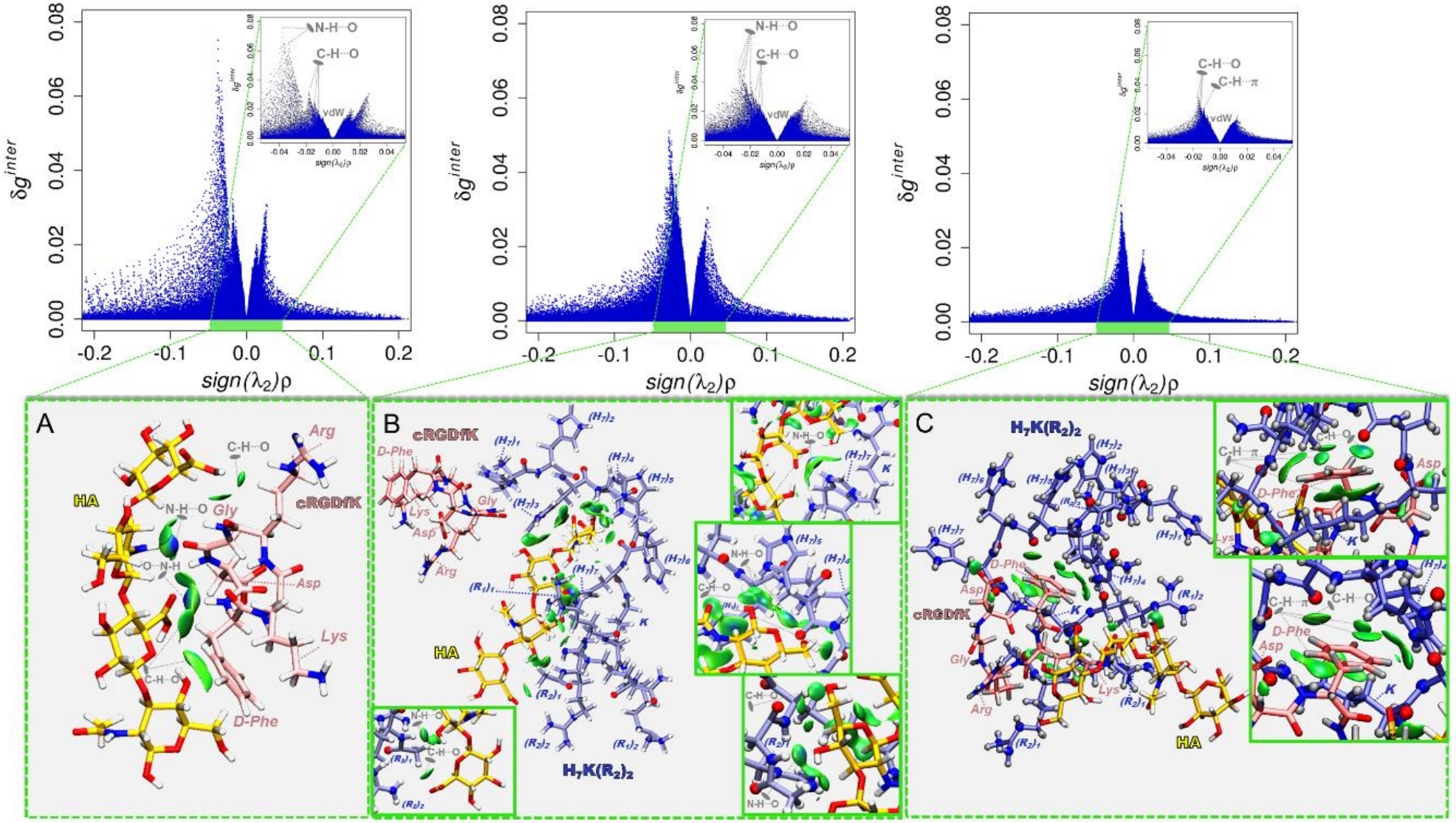
δg^inter
sign(λ2)ρ
N-H···O
C-H···O
C-H···π
vdW
A
HA
cRGDfK
Arg
Gly
Asp
Lys
D-Phe
B
H7K(R2)2
C

Figure 9. Interaction patterns underlying polymer/peptides association (A) HA-c(RGDfK), (B) HA-c(RGDfK)-$H_7K(R_2)_2$, and (C) HA-c(RGDfK):$H_7K(R_2)_2$, represented in the 2D scatter plots (top) and in the 3D IGMPlot isosurfaces (bottom). The coordinates corresponding to the final conjugate structures were extracted from the last time step of MD simulations. Isosurfaces display the total IGM interaction points for $\delta g_{inter} \leq 0.1$ and in the region $-0.2 \leq sign(\lambda_2)\rho \leq 0.2$. and are colored based on a red-green-blue gradient over the electron density range $-0.05 < sign(\lambda_2)\rho < 0.05$ a.u.. Blue/red reflect stabilizing/destabilizing noncovalent interactions, while green represents van der Waals-type forces. HA and c(RGDfK) backbones are represented in yellow and pink, respectively, as licorice, while $H_7K(R_2)_2$ is featured in ball-and-stick and colored in iceblue. Nitrogen, oxygen and hydrogen atoms are represented in blue, red and white, respectively.

Table S10 summarizes the atom interaction pairs in each of the peptide constructs. The stability of the H-c(RGDfK) conjugate (**Figure 9, panel A**) is essentially governed by two N-H···O hydrogen-bonds (represented by large volumes with blue centers), as also suggested in **Figure 8**, and also by C-H···O type interactions. Such observations are consistent with the previous NMR results, see **Figure 7**. N-H···O interactions are also depicted as large diffuse peaks (ca. 2 N-H···O hydrogen-bonds in HA:c(RGDfK), **panel A**, and at least 4 N-H···O hydrogen-bonds in HA:$H_7K(R_2)_2$, panel B, with the respective maxima defined at $-0.05<sign(\lambda_2)\rho<-0.02$. In the presence of $H_7K(R_2)_2$, no interactions were found between HA and c(RGDfK) or $H_7K(R_2)_2$ and c(RGDfK) (**panel B**). This suggests a competition effect between both peptides and a higher affinity of HA to $H_7K(R_2)_2$. The type of hydrogen-bonds in panels A and B are similar, although the N-H···O involving the histidine and arginine residues of $H_7K(R_2)_2$ and both glucuronic acid and N-acetylglucosamine moieties of HA are less pronounced. These hydrogen-bonds are identified as the larger diffuse peaks at $sign(\lambda_2)\rho\approx$ -0.03 in the corresponding 2D scatter plot. There are also additional well-defined peaks corresponding to the C-H···O interactions established for e.g. between (i) CH_3- group of arginine $(R_2)_1$ and the carboxyl group of glucuronic acid (ii) histidine $(H_7)_3$ and the acetyl group of N-acetylglucosamine (**Figure 7, panel B**). Interestingly, these observations suggest that the introduction of the $H_7K(R_2)_2$ in the system containing the unmodified HA (panel B) prevents the interaction between HA and c(RGDfK), since the affinity between HA and $H_7K(R_2)_2$ prevails. : In the absence of interaction with c(RGDfK), and the close proximity of the HA and $H_7K(R_2)_2$ binding partners support, as previously suggested, the preformation of the HA-c(RGDfK) structure involving the carboxyl group of glucuronic acid and the c(RGDfK)-lysine terminal NH_2, so as to obtain a stable ternary conjugate. Similar conjugation of HA with amines has previously been proposed[25,40]. Although lysine and arginine have the possibility of hydrogen bond formation with the carboxylic groups through their terminal NH_2 groups, bonding involving lysine is more likely, based on the pKa values of the lateral N-H groups, 10.5 and 13.8, respectively[41,42]. Once again, such interaction patterns confirm the previous findings seen in the NMR spectra and the respective estimated coupling constants.

In addition to the multiple N-H···O hydrogen-bonds derived from the $H_7K(R_2)_2$ (N-H) :HA(O) interactions, the HA:$H_7K(R_2)_2$ binding is also favored by slightly enhanced van der Waals interactions, depicted as flat green regions. In contrast to HA:$H_7K(R_2)_2$ (panel B), in HA-c(RGDfK):$H_7K(R_2)_2$ (**panel C**), the weakly stabilizing

van der Waals-type interactions are established mainly between the $H_7K(R_2)_2$-lysine (K) moiety and the c(RGDfK)-phenylalanine phenyl CH groups. Stabilization of the HA-c(RGDfK):$H_7K(R_2)_2$ construct is also assured by weak hydrogen bonds between the $H_7K(R_2)_2$-arginine (R_1 and R_2) carbonyl groups, and the c(RGDfK)-lysine $C_\varepsilon H_2$, $C_\beta H_2$, $C_\gamma H_2$ and c(RGDfK)-aspartate $C_\beta H_2$ groups.

The architecture of HA-c(RGDfK):$H_7K(R_2)_2$ also exhibits propensity to establish hydrophobic C-H···C-H interactions and C-H···π dispersion interactions (**Figure 9, panel C**). These support the decrease of flexibility previously observed due to the formation of a "pocket-like" conformation.

For the former, the C-H bonds belong for e.g. to the $H_7K(R_2)_2$-arginine $(R_2)_1$ and c(RGDfK)-lysine ($C_\gamma H_2$). C-H···π interactions are established between the $H_7K(R_2)_2$-lysine(K) moiety, which acts as C-H donor, and the electron-rich phenyl ring of c(RGDfK)-phenylalanine moiety, which corresponds to the π system (**panel C**). These interactions can also be identified in the more intense peaks on the left, at $sign(\lambda_2)\rho \approx$ -0.016. Such weak attractive forces have been recognized as important driving forces in the association process of similar systems involving carbohydrates and aromatic moieties, and also protein-drug complexes[33,43–45]. Some energy calculations have also suggested that the center of the phenyl ring acts as a hydrogen bond acceptor and that the interaction with the hydrogen donor is half the strength of a typical hydrogen bond, contributing with approximately 12.6 kJ/mol of stabilizing enthalpy[46].

Decomposition of the individual atomic contributions in HA-c(RGDfK):$H_7K(R_2)_2$, as well as estimation of the impact of a specific polymer/peptide atom in the intermolecular region between the binding partners is also provided by the IGM analysis, as a complementary information (**Figure 10**). Different contact patterns are observed due to distinct contributions of the polymer-peptide atoms, either in the well-defined larger volumes corresponding to hydrogen bonds or in the flat isosurfaces representing the hydrophobic, van der Waals and dispersion interactions. The atoms of the final conjugate are depicted in a gray (no contribution)-to-red (high relative contribution) color scheme, following the impact on the isosurfaces of **Figure 10**. An accurate estimation of the contribution, expressed in a percentage score, of each polymer-peptide atom in the pro-molecular electron density gradient, displayed in the peaks of the δg_{inter} vs. $sign(\lambda_2)\rho$ plot, is thus provided. Establishing individual atom contributions in the formation of these conjugates allows understanding the molecular determinants of polymer-peptide and peptide-peptide recognition.

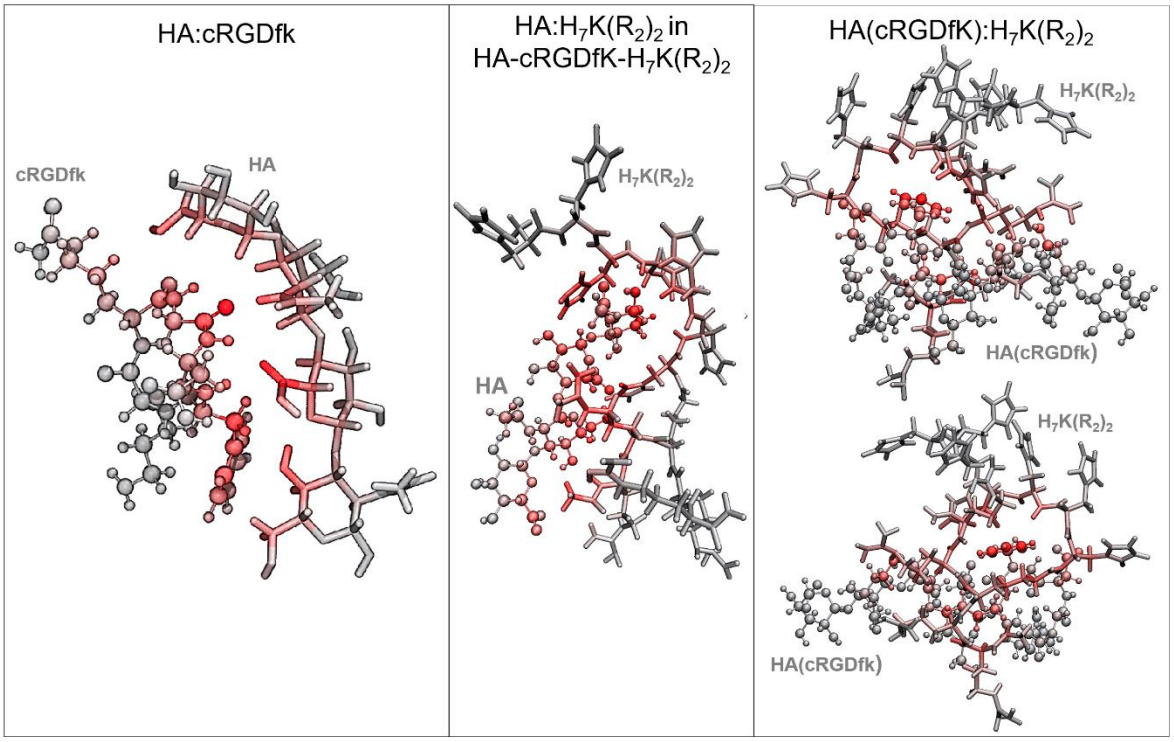

Figure 10. Representative conformations of polymer-peptide conjugates showing the individual atom contributions to the polymer-peptide noncovalent interactions, which are discriminated in the isosurfaces represented in **Figure 9**. Each atom is colored using a gray (no contribution)-to-red (significant relative contribution) gradient reflecting the relative score (%).

4. Conclusions

Keeping active targeting and also nanoparticle surface modulation purposes in consideration, a hybrid polymer-peptide construct based on HA as biopolymer, and c(RGDfK) and $H_7K(R_2)_2$ as peptides was successfully designed. The establishment of such molecular assemblies was comprehensively characterized based on NMR and MD simulations. While NMR provided evidenced regarding structured architecture, MD simulation shed light on the relevant contacts between the interaction pairs. These methodologies enabled to set forth a hierarchy in terms of synthesis pathway, governed by the size and amino acid residue rearrangement, and also the appropriate molar ratio (1:1) required to obtain a favorable system ultimately able to interact with the tumor cell membrane. Current ongoing in vitro/in vivo studies have been performed to set forth the proof-of-concept of hierarchical targeted nanosystem.

Acknowledgments

The authors acknowledge the Portuguese Agency for Scientific Research, "Fundação para a Ciência e a Tecnologia (FCT)", for the financial support through the projects POCI-01-0145-FEDER-016648, PEst-UID/NEU/04539/2013 and COMPETE (Ref. POCI-01-0145-FEDER-007440). The Coimbra Chemistry Centre (CQC) is also supported by FCT through the Project UID/QUI/00313/2020. RV also acknowledges FCT for the financial support of the projects IF/00286/2015, iBiMED (UID/BIM/04501/2019 and POCI-01-0145-FEDER-007628), and UnIC (UID/IC/00051/2019). Maria Mendes and João Basso acknowledge the PhD research Grants SFRH/BD/133996/2017 and SFRH/BD/149138/2019, respectively, assigned by FCT.

NMR data were obtained at the UC-NMR facility which is supported in part by the FEDER – European Regional Development Fund through the COMPETE Programme (Operational Programme for Competitiveness) and by the National Funds through FCT with the grants REEQ/481/QUI/2006, RECI/QEQ- QFI/0168/2012, CENTRO-07-CT62-FEDER-002012, and the Rede Nacional de Ressonância Magnética Nuclear (RNRMN).

References

1 T. Kazda, A. Dziacky, P. Burkon, P. Pospisil, M. Slavik, Z. Rehak, R. Jancalek, P. Slampa, O. Slaby and R. Lakomy, *Radiol. Oncol.*, 2018, **52**, 121–128.

2 R. Stupp, W. P. Mason, M. J. Van Den Bent, M. Weller, B. Fisher, M. J. B. Taphoorn, K. Belanger, A. A. Brandes, C. Marosi and U. Bogdahn, *N. Engl. J. Med.*, 2005, **352**, 987–996.

3 H. P. Ellis, M. Greenslade, B. Powell, I. Spiteri, A. Sottoriva and K. M. Kurian, *Front. Oncol.*, 2015, **5**, 251.

4 O. Van Tellingen, B. Yetkin-Arik, M. C. De Gooijer, P. Wesseling, T. Wurdinger and H. E. De Vries, *Drug Resist. Updat.*, 2015, **19**, 1–12.

5 K. B. Johnsen, A. Burkhart, F. Melander, P. J. Kempen, J. B. Vejlebo, P. Siupka, M. S. Nielsen, T. L. Andresen and T. Moos, *Sci. Rep.*, 2017, **7**, 10396.

6 M. Mendes, J. Sousa, A. Pais and C. Vitorino, *Pharmaceutics*, 2018, **10**, 181.

7 K. K. Jain, *Front. Oncol.*

8 L. Zhang, Y. Zhang, L. Tai, K. Jiang, C. Xie, Z. Li, Y.-Z. Lin, G. Wei, W. Lu and W. Pan, *Acta Biomater.*, 2016, **42**, 90–101.

9 H. Gao, S. Zhang, S. Cao, Z. Yang, Z. Pang and X. Jiang, *Mol. Pharm.*, 2014, **11**, 2755–2763.

10 W. Ke, Z. Zha, J. F. Mukerabigwi, W. Chen, Y. Wang, C. He and Z. Ge, *Bioconjug. Chem.*, 2017, **28**, 2190–2198.

11 T. J. Harris, G. von Maltzahn, M. E. Lord, J. Park, A. Agrawal, D. Min, M. J. Sailor and S. N. Bhatia, *small*, 2008, **4**, 1307–1312.

12 J. Yao, Y. Ma, W. Zhang, L. Li, Y. Zhang, L. Zhang, H. Liu, J. Ni and R. Wang, *PeerJ*, 2017, **5**, e3429.

13 K. Shi, Y. Long, C. Xu, Y. Wang, Y. Qiu, Q. Yu, Y. Liu, Q. Zhang, H. Gao and Z. Zhang, *ACS Appl. Mater. Interfaces*, 2015, **7**, 21442–21454.

14 Y. Wang, K. Shi, L. Zhang, G. Hu, J. Wan, J. Tang, S. Yin, J. Duan, M. Qin and N. Wang, *Autophagy*, 2016, **12**, 949–962.

15 T. Jiang, Z. Zhang, Y. Zhang, H. Lv, J. Zhou, C. Li, L. Hou and Q. Zhang, *Biomaterials*, 2012, **33**, 9246–9258.

16 H. Zhou, H. Xu, X. Li, Y. Lv, T. Ma, S. Guo, Z. Huang, X. Wang and P. Xu, *Mater. Sci. Eng. C*, 2017, **81**, 261–270.

17 M. Swierczewska, H. S. Han, K. Kim, J. H. Park and S. Lee, *Adv. Drug Deliv. Rev.*, 2016, **99**, 70–84.

18 L. I. Qin, C. Wang, H. Fan, C. Zhang, H. Zhang, M. Lv and S. Cui, *Oncol. Lett.*, 2014, **8**, 2000–2006.

19 S. Song, G. Mao, J. Du and X. Zhu, *Drug Deliv.*, 2016, **23**, 1404–1408.

20 Y. Miura, T. Takenaka, K. Toh, S. Wu, H. Nishihara, M. R. Kano, Y. Ino, T. Nomoto, Y. Matsumoto and H. Koyama, *ACS Nano*, 2013, **7**, 8583–8592.

21 H. Hyun, Y. Yoo, S. Y. Kim, H. S. Ko, H. J. Chun and D. H. Yang, *J. Ind. Eng. Chem.*, 2020, **81**, 178–184.

22 M. Zhou, N. Jiang, J. Fan, S. Fu, H. Luo, P. Su, M. Zhang, H. Shi, J. Zeng and Y. Huang, *J. Control. Release*, 2019, **310**, 24–35.

23 Y. Zhao, W. Ren, T. Zhong, S. Zhang, D. Huang, Y. Guo, X. Yao, C. Wang, W.-Q. Zhang and X. Zhang, *J. Control. Release*, 2016, **222**, 56–66.

24 D. Gfeller, A. Grosdidier, M. Wirth, A. Daina, O. Michielin and V. Zoete, *Nucleic Acids Res.*, 2014, **42**, W32–W38.

25 Z. R. Cohen, S. Ramishetti, N. Peshes-Yaloz, M. Goldsmith, A. Wohl, Z. Zibly and D. Peer, *ACS Nano*, 2015, **9**, 1581–1591.

26 P. K. Glasoe and F. A. Long, *J. Phys. Chem.*, 1960, **64**, 188–190.

27 T. F. G. G. Cova, D. J. Bento and S. C. C. Nunes, *Pharmaceutics*, 2019, **11**, 119.

28 A. Aviñó, A. F. Jorge, C. S. Huertas, T. F. G. G. Cova, A. Pais, L. M. Lechuga, R. Eritja and C. Fabrega, *Biochim. Biophys. Acta (BBA)-General Subj.*, 2019, **1863**, 1619–1630.

29 M. Mendes, A. Miranda, T. Cova, L. Gonçalves, A. J. Almeida, J. J. Sousa, M. L. C. do Vale, E. F. Marques, A. Pais and C. Vitorino, *Eur. J. Pharm. Sci.*, 2018, **117**, 255–269.

30 A. Jakalian, B. L. Bush, D. B. Jack and C. I. Bayly, *J. Comput. Chem.*, 2000, **21**, 132–146.

31 D. Van Der Spoel, E. Lindahl, B. Hess, G. Groenhof, A. E. Mark and H. J. C. Berendsen, *J. Comput. Chem.*, 2005, **26**, 1701–1718.

32 V. Hornak, R. Abel, A. Okur, B. Strockbine, A. Roitberg and C. Simmerling, *Proteins Struct. Funct. Bioinforma.*, 2006, **65**, 712–725.

33 T. F. Cova, B. F. Milne and A. A. C. C. Pais, *Carbohydr. Polym.*, 2019, **205**, 42–54.

34 J. Wong-ekkabut and M. Karttunen, *Biochim. Biophys. Acta (BBA)-Biomembranes*, 2016, **1858**, 2529–2538.

35 B. Hess, H. Bekker, H. J. C. Berendsen and J. G. E. M. Fraaije, *J. Comput.*

Chem., 1997, **18**, 1463–1472.
36 C. Lefebvre, G. Rubez, H. Khartabil, J.-C. Boisson, J. Contreras-García and E. Hénon, *Phys. Chem. Chem. Phys.*, 2017, **19**, 17928–17936.
37 L. M. P. Verissimo, J. M. M. Teigão, M. L. Ramos, H. D. Burrows, M. A. Esteso and A. C. F. Ribeiro, *J. Chem. Thermodyn.*, 2016, **101**, 245–250.
38 M. C. F. Barros, M. L. Ramos, H. D. Burrows, M. A. Esteso, D. G. Leaist and A. C. F. Ribeiro, *J. Chem. Thermodyn.*, 2015, **90**, 169–173.
39 H. Tian, L. Lin, J. Chen, X. Chen, T. G. Park and A. Maruyama, *J. Control. release*, 2011, **155**, 47–53.
40 R. D. Dubey, R. Klippstein, J. T.-W. Wang, N. Hodgins, K.-C. Mei, J. Sosabowski, R. C. Hider, V. Abbate, P. N. Gupta and K. T. Al-Jamal, *Nanotheranostics*, 2017, **1**, 59.
41 M. J. Harms, J. L. Schlessman, M. S. Chimenti, G. R. Sue, A. Damjanović and B. García- Moreno E, *Protein Sci.*, 2008, **17**, 833–845.
42 C. A. Fitch, G. Platzer, M. Okon, B. Garcia- Moreno E and L. P. McIntosh, *Protein Sci.*, 2015, **24**, 752–761.
43 T. F. G. G. Cova, S. C. C. Nunes and A. A. C. C. Pais, *Phys. Chem. Chem. Phys.*, 2017, **19**, 5209–5221.
44 M. Nishio, *Phys. Chem. Chem. Phys.*, 2011, **13**, 13873–13900.
45 V. Spiwok, *Molecules*, 2017, **22**, 1038.
46 M. Levitt and M. F. Perutz, *J. Mol. Biol.*, 1988, **201**, 751–754.

Author statement

Maria Mendes: Investigation, Writing - Original Draft Tânia Cova: Data Curation, Writing - Original Draft, Formal Analysis, João Basso: Writing - Original Draft, Validation, Maria Luísa Ramos: Investigation, Data Curation, Writing - Original Draft, Formal Analysis, Rui Vitorino: Software, Reviewing, João Sousa: Resources, Supervision, Alberto Pais: Resources, Supervision, Editing & Reviewing Carla Vitorino: Conceptualization, Writing- Reviewing and Editing

Declaration of interests

☒ The authors declare that they have no known competing financial interests or personal relationships that could have appeared to influence the work reported in this paper.

☐The authors declare the following financial interests/personal relationships which may be considered as potential competing interests:

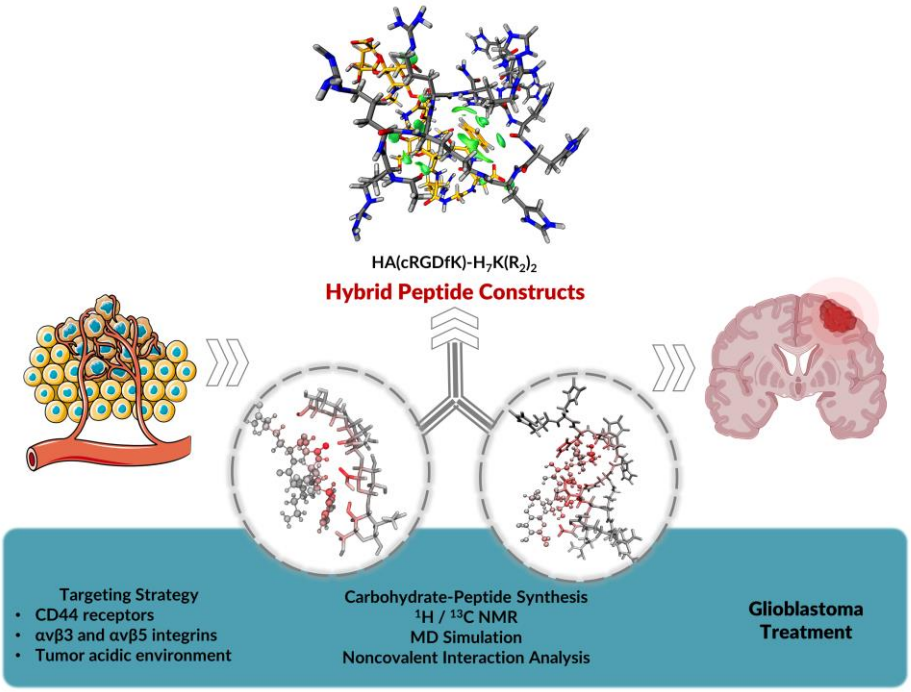

Graphical abstract

Highlights

A hybrid construct based on HA, c(RGDfK) and $H_7K(R_2)_2$ is successfully designed.

A dual experimental-computational framework is provided for guiding conjugate formation.

MD enlightens the interactions governing the formation and stability of the constructs.

Synthesis pathway requires a hierarchical conjugation of the HA-c(RGDfK)-H7k$(R_2)_2$.

HA-c(RGDfK)-H7k$(R_2)_2$ conjugate displays a promising tumor targeting signature.